Title	Synthesis and solution properties of a rigid helical star polymer: Three-Arm Star Poly(quinoxaline-2,3-diyl)
Author(s)	Hasegawa, Hirokazu; Nagata, Yuuya; Terao, Ken et al.
Citation	Macromolecules. 2017, 50(19), p. 7491-7497
Version Type	AM
URL	https://hdl.handle.net/11094/81801
rights	This document is the Accepted Manuscript version of a Published Work that appeared in final form in Macromolecules, © American Chemical Society after peer review and technical editing by the publisher. To access the final edited and published work see https://doi.org/10.1021/acs.macromol.7b01797.
Note	

Osaka University Knowledge Archive : OUKA

https://ir.library.osaka-u.ac.jp/

Osaka University

Synthesis and Solution Properties of a Rigid Helical Star Polymer: Three-arm Star Poly(quinoxaline-2,3-diyl)

Hirokazu Hasegawa,[†,‡] Yuuya Nagata,*[§] Ken Terao,*[†] and Michinori Suginome[§]

[†]Department of Macromolecular Science, Graduate School of Science, Osaka University, 1-1 Machikaneyama-cho, Toyonaka, Osaka 560-0043, Japan
[‡]Materials Characterization Laboratories, Toray Research Center, Inc., 3-3-7, Sonoyama, Otsu, Shiga 520-8567, Japan
[§]Department of Synthetic Chemistry and Biological Chemistry, Graduate School of Engineering, Kyoto University, Katsura, Kyoto 615-8510, Japan

Corresponding Authors
* E-mail: nagata@sbchem.kyoto-u.ac.jp
* E-mail: kterao@chem.sci.osaka-u.ac.jp

ABSTRACT: Six semiflexible helical three-arm star poly[5,8-dimethyl-6,7-bis(propoxymethyl)quinoxaline-2,3-diyl] (A3PQ) samples which have different arm length ranging in the weight-average molar mass M_w from 1.5×10^4 g mol^{-1} to 2.5×10^5 g mol^{-1} were synthesized via the living polymerization of the corresponding 1,2-diisocyanobenzene using a trifunctional palladium initiator. The particle scattering function $P(q)$, the z-average mean-square radius of gyration $\langle S^2 \rangle_z$, and the intrinsic viscosity $[\eta]$ for the A3PQ samples were determined from light and small-angle X-ray scattering and viscosity measurements in tetrahydrofuran at 25 °C. The obtained data were compared with modern theories for the wormlike star. The experimental $P(q)$ data were represented by the wormlike star model connected with a universal joint. The other data were comparably explained by the same model.

Introduction

Star polymers are a class of simple non-linear polymers. Well-defined star polymers consisting of flexible arms are thoroughly investigated both theoretically and experimentally.[1-2] Conformational properties of stiff polymer chains are more readily to be understood theoretically since intramolecular excluded-volume effects are much less important than those for the flexible polymer chains.[3] Experimental researches to determine gyration radii and/or intrinsic viscosities of semiflexible or rigid star polymers are however limited to poly(γ-benzyl-L-glutamate),[4] poly(*n*-hexylisocyanate),[5-6] and specially designed 'polypod' DNA.[7] Polymer conformations of such star polymers are important to understand their structure-function relationships if we consider some star polymers with rigid (helical) arms are considerably attractive because of their unique features, that is, molecular recognition[8] and self-assembly behavior.[9-11] Quantitative discussion of dimensional and hydrodynamic properties in terms of the modern theories[12] are however limited. Taking into account that the heterogeneity of the main chain and relatively large core of the star polymers significantly influence their dimensional properties as seen in a triple helical peptide with a linker domain,[13] star polymers consisting of rigid homopolymer and well defined core are indispensable to clarify conformational features of semiflexible stars.

We thus synthesized a three-arm star polymer (A3PQ) having rigid helical poly[5,8-dimethyl-6,7-bis(propoxymethyl)quinoxaline-2,3-diyl] (PQX) with a well-designed three-functional initiator. A linear PQX behaves as a semi-rigid polymer of which Kuhn segment length (λ^{-1}) was reported to be 43 nm in tetrahydrofuran (THF) at 25 °C.[14] It is thus a candidate as a unique class of functional polymers because linear poly(quinoxaline-2,3-diyl)s are useful as highly effective chiral ligands for transition metal catalysts in asymmetric reactions,[15] and furthermore, they may have solvent dependent helix reversal behaviors.[16-17] We prepared A3PQ samples with different molar mass. Light scattering, small-angle X-ray scattering, and viscosity measurements were made for the samples in THF to determine their dimensional and hydrodynamic properties. The resultant solution data were analyzed in terms of the modern theories for wormlike stars to clarify their molecular conformation in solution.
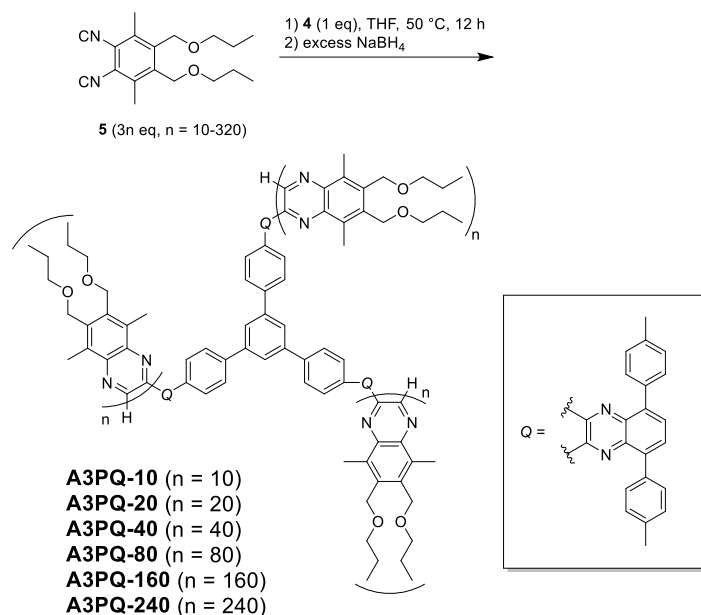
Experimental Section

Synthesis of A3PQ. Six A3PQ samples were synthesized by the core first method as shown in Schemes 1 and 2. All reactions were carried out under a nitrogen atmosphere. 1,3,5-Tris-(4-iodo-phenyl)-benzene (**1**),[18] 1,2-diisocyano-3,6-di-*p*-tolylbenzene (**3**),[19] and 1,2-diisocyano-3,6-dimethyl-4,5-bis(propoxymethyl)benzene (**5**)[20] were prepared according to the reported procedures. Other chemical reagents were purchased from the commercial sources and were used without further purification.

Scheme 1. Synthesis of the trifunctional palladium initiator **4**.
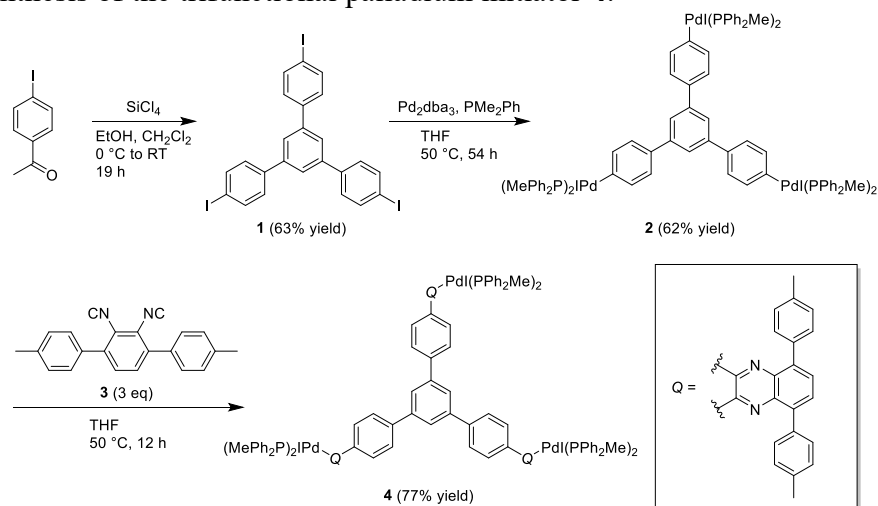
Scheme 2. Polymerization of 1,2-dicyanobenzene monomer **5** with the trifunctional palladium initiator **4**.

5 (3n eq, n = 10-320)

1) 4 (1 eq), THF, 50 °C, 12 h
2) excess NaBH₄

A3PQ-10 (n = 10)
A3PQ-20 (n = 20)
A3PQ-40 (n = 40)
A3PQ-80 (n = 80)
A3PQ-160 (n = 160)
A3PQ-240 (n = 240)

$Q =$

A procedure to synthesize a trifunctional palladium initiator **4** is as follow: Tris(dibenzylideneacetone)dipalladium(0) (Pd$_2$dba$_3$, 1.30 g, 1.42 mmol) and dimethylphenylphosphine (PMe$_2$Ph, 0.82 mL, 5.79 mmol) were dissolved in THF (5.85 mL) and stirred for 10 min. A THF solution of **1** (0.4 g, 0.584 mmol in 11.69 mL of THF) was added to the reaction mixture and stirred at 50 °C for 54 h. After the reaction, the reaction mixture was filtered through a pad of Celite and washed with dichloromethane (CH$_2$Cl$_2$, 50 mL). The filtrate was concentrated under reduced pressure. The residual brown solid was subjected to a silica gel column chromatography using CH$_2$Cl$_2$ as an eluent (R_f = 0.42 using CH$_2$Cl$_2$). After evaporation to dryness, the crude product was dissolved in CH$_2$Cl$_2$ (5 mL) and reprecipitated into methanol (50 mL). The precipitate was washed with methanol (50 mL) and dried under vacuum to give white solid of **2** (0.66 g, 62% yield). Compounds **2** (0.300 g, 0.164 mmol) and **3** (0.152 g, 0.491 mmol) were dissolved in THF (9.8 mL). The reaction mixture was stirred at 50 °C for 24 h. After evaporation of the reaction mixture to dryness, the residual solid was subjected to a silica gel column chromatography using n-hexane and CH$_2$Cl$_2$ (n-hexane/ CH$_2$Cl$_2$ = 25/75 to 0/100, R_f = 0.50 using n-hexane/ CH$_2$Cl$_2$ = 25/75) to give **4** as a yellow solid (0.35 g, 77% yield).

A typical procedure for the polymerization is as follows: **A3PQ-40**: Compound **4** (0.0129 mol/L, 0.71 mL) was added to a solution of **5** (0.1271 g, 0.4232 mmol) in THF (16.9 mL). The reaction mixture was stirred at 50 °C. After 12 h, excess amount of NaBH$_4$ (0.0534 g, 1.41 mmol) was added, and the reaction mixture was stirred for 2 h at room temperature. The resultant mixture was poured into water (50 mL) and extracted with chloroform (50 mL × 3). The organic extract was dried over MgSO$_4$, and the solvent was evaporated. The residue was subjected to preparative size exclusion chromatography (SEC) to give **A3PQ-40** as a brown solid (126.5 mg, 96% yield). Six A3PQ samples, **A3PQ-10**, **A3PQ-20**, **A3PQ-40**, **A3PQ-80**, **A3PQ-160**, and **A3PQ-240** of which weight-average molar mass M_w ranges from 1.5×10^4 g mol^{-1} to 2.5×10^5 g mol^{-1} were eventually prepared for this study. The chemical structures of the resultant polymer and the initiator were confirmed by ^{1}H NMR and/or X-ray analysis as reported in the Supporting Information.

3

Static Light Scattering (SLS) and Viscosity Measurements with SEC. SLS and viscosity measurements for all samples in THF were made using SEC equipped with a DAWN HELEOS multi-angle laser light scattering photometer, an Optilab rEX differential refractometer, and a VISCOSTAR-II differential viscometer (Wyatt Technology, USA) at room temperature (~ 25 °C). Two TSKgel GMH$_{XL}$ columns and a G2500H$_{XL}$ column connected in series were used for the SEC system. Details of the experimental and analytical procedures were the same as those for the corresponding linear PQX as mentioned previously.[14] Differential refractive index increments $\partial n/\partial c$ for all A3PQ samples in THF at the wavelength in vacuum (λ_0) of the light scattering photometer were determined by using the peak area of the refractive index chromatogram and the polymer mass concentration c of injected solution assuming full recovery of the A3PQ sample. The $\partial n/\partial c$ value was also determined for **A3PQ-80** with an Optilab T-rEX differential refractometer (Wyatt) by a batch method to be 0.192 cm^{3}g^{-1}, which is the same as that from the former method. The weight-average molar mass M_w, the intrinsic viscosity $[\eta]$, and the z-average mean-square radius of gyration $\langle S^2 \rangle_z$ for the A3PQ samples were determined at each retention volume V_e. We note that the light scattering data were analyzed in terms of the Berry square-root plot[21] and the values of $\langle S^2 \rangle_z$ were not determined for **A3PQ-10**, **A3PQ-20**, **A3PQ-40**, and **A3PQ-80** because they were less than the lower limit (~ 100 nm^2) of the light scattering detector. The resultant M_w values determined from the peak area agreed with those from the universal calibration method[22-23] within ± 3%. The dispersity index $Đ$ defined as the ratio of M_w to the number average molar mass M_n from the two methods was also determined from the two methods. The SEC chromatograms for **A3PQ-80**, **A3PQ-160**, and **A3PQ-240** have a small shoulder peak suggesting high molar mass component as displayed in Figure 1. Similar component was also observed for the linear PQX samples.[14] The shoulder peaks were thus omitted in the following analyses.
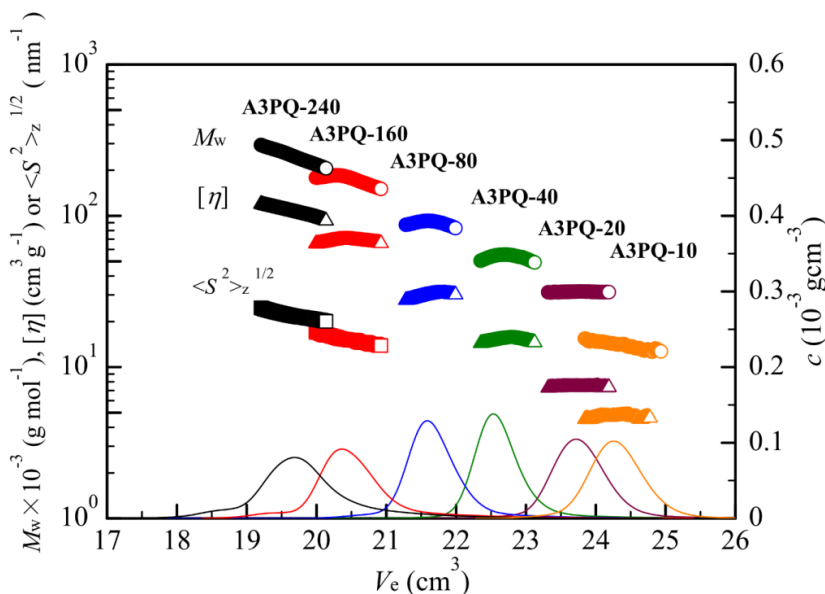

Figure 1. Retention volume V_e dependence of the weight-average molar mass M_w (circles), the z-average radius of gyration $\langle S^2 \rangle_z^{1/2}$ (squares), the intrinsic viscosity $[\eta]$ (triangles), and the polymer mass concentration c (solid curves) for the indicated A3PQ samples in THF at room temperature (~ 25 °C).

Small angle X-ray Scattering (SAXS).   SAXS measurements were performed for **A3PQ-10**, **A3PQ-20**, **A3PQ-40**, **A3PQ-80**, and **A3PQ-160** in THF at 25 °C using a Rigaku R-AXIS VII imaging plate at the BL40B2 beamline in SPring-8 (Hyogo, Japan). The camera length, λ_0, and the accumulation time were set to be 4 m, 0.1 nm, and 180 sec, respectively. The magnitude q of the scattering vector at each pixel was determined from the diffraction pattern of silver behenate. The measurements were carried out for the solvent and four solutions having different c ranging in 6×10^{-3} g cm^{-3} and 3×10^{-2} g cm^{-3}. The scattering intensity $I(q)$ was obtained as a function of q by the circular average procedure. The excess scattering intensity $\Delta I(q)$ of each solution was determined from the difference between $I(q)$ of the solution and that of the solvent in the same capillary cell taking the intensity and transparency of the incident X-ray into account. The $[c/\Delta I(q)]^{1/2}$ data were extrapolated to infinite dilution and to $q^2 = 0$ to estimate the particle scattering function $P(q)$.   Figure 2 shows the Berry plot of the resultant $P(q)$ data to determine $\langle S^2 \rangle_z$. Since the extrapolation to $q^2 = 0$ was infeasible for **A3PQ-160**, we estimated the $P(q)$ to fit the experimental data at the lowest q to the dashed line of which initial slope was drawn to represent the $\langle S^2 \rangle_z$ value determined from light scattering measurements.
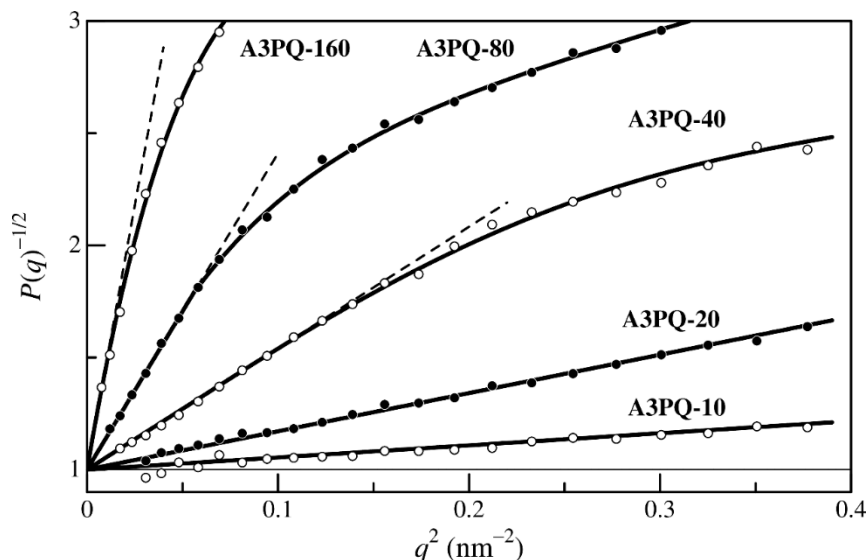

Figure 2. Berry square-root plots for indicated A3PQ samples in THF at 25 °C. Dashed lines indicate the initial slopes.

Results

Table 1 summarizes numerical data for $\partial n/\partial c$, M_w, $Đ$ ($\equiv M_w/M_n$), $<S^2>_z$, and $[\eta]$ mainly determined from the above mentioned SEC and SAXS measurements. The quite small $Đ$ values for the A3PQ samples suggest the relatively narrow arm length distribution while direct observation has not been examined. The $\partial n/\partial c$ values for the two lowest M_w samples, **A3PQ-10** and **A3PQ-20**, are somewhat larger than those for the higher molar mass samples. This is most likely due to the higher refractive index of the core region.

Table 1. Molecular Characteristics of Three-arm Star Poly[5,8-dimethyl-6,7-bis(propoxymethyl)quinoxaline-2,3-diyl] (A3PQ) Samples and Physical Properties in THF at 25 °C or Room Temperature (~25 °C)

Sample	$\partial n/\partial c$ (cm^3 g^{-1})	M_w (10^{-3} g mol^{-1})	$Đ$ (M_w / M_n)	$\langle S^2 \rangle_z^{1/2}$ (nm)	$[\eta]$ (cm^3 g^{-1})	g_s	g_η
A3PQ-10	0.207	14.8	1.01 [b] 1.09 [c]	1.8 [a]	4.8	0.51	0.69
A3PQ-20	0.199	31.9	1.01 [b] 1.15 [c]	3.2 [a]	7.3	0.38	0.47
A3PQ-40	0.190	52.9	1.06 [b] 1.18 [c]	5.7 [a]	14.4	0.48	0.53
A3PQ-80	0.192	88.8	1.04 [b] 1.08 [c]	9.1 [a]	29.0	0.51	0.58
A3PQ-160	0.189	176	1.07 [b] 1.19 [c]	16.8 [b]	67.0	0.60	0.62
A3PQ-240	0.187	245	1.18 [b] 1.16 [c]	22.0 [b]	103	0.65	0.67

[a] From SAXS. [b] From SEC-SLS. [c] From universal calibration.

Molar mass dependence of the resultant $\langle S^2 \rangle_z^{1/2}$ data for the A3PQ samples are illustrated in Figure 3. They are systematically smaller than those for the corresponding linear polymer. The factor g_s defined as

$$g_s = \frac{\langle S^2 \rangle_{star}}{\langle S^2 \rangle_{linear}}$$

(1)

was calculated using the theoretical values for the corresponding linear chain.[14] The resultant g_s values are listed in the 7th column in Table 1. These values are between 1/3 and 7/9 for rod like and Gaussian three arm stars, respectively (see later). The Holtzer plot of $P(q)$ has an appreciable peak at low q region and it becomes mostly flat with increasing q as illustrated in Figure 4 while such peak was not seen in those for the corresponding linear chain.[14] This is most likely due to the smaller dimensions of the star polymers than those for the corresponding linear chain with the same M_w.
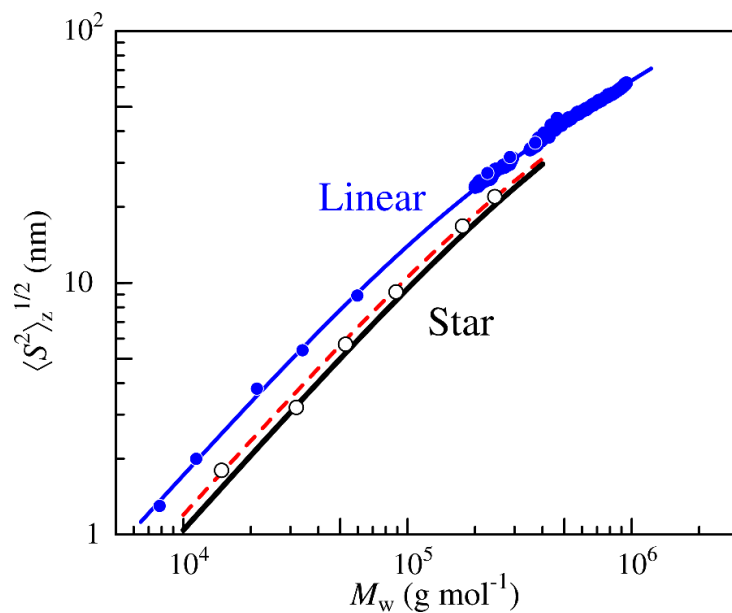
Figure 3. Double logarithmic plots of $\langle S^2 \rangle_z^{1/2}$ vs M_w for A3PQ (unfilled circles) and PQX (filled circles) in THF at 25 °C or the room temperature. Solid black and dashed red curves indicate the broken ($\langle S^2 \rangle_{BW}$, eq 9) and fixed ($\langle S^2 \rangle_{FIX}$, eq 10) wormlike chains, respectively, with the parameters shown in the text.
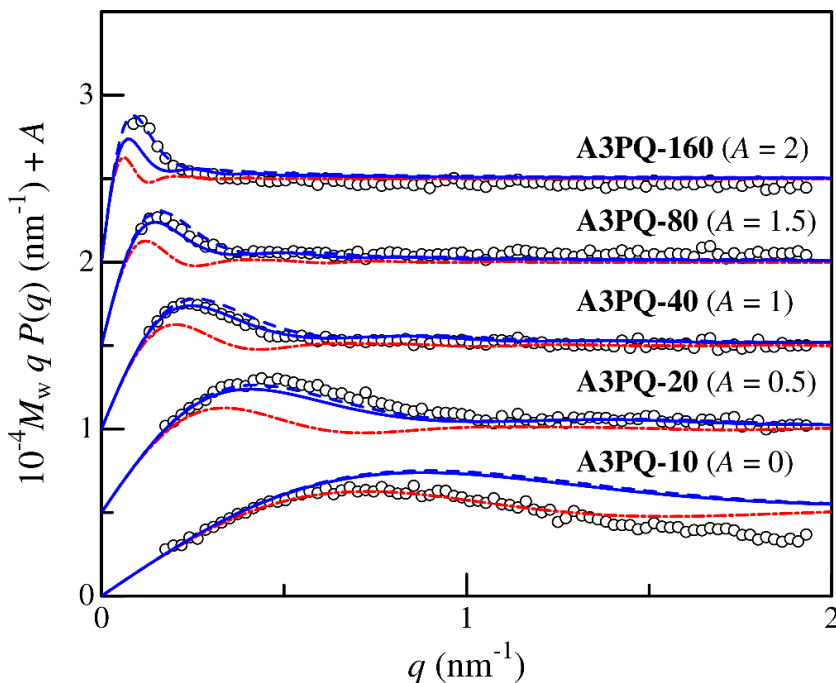

Figure 4. Reduced Holtzer plots for the indicated A3PQ samples in THF at 25 °C. Solid and dashed blue curves denote the theoretical values for the rigid [$P_{BR}(q)$, eq 3] and wormlike [$P_{BW}(q)$, eq 8] broken star, respectively, with the parameters written in the text. The dot-dashed red curves represent the theoretical values of the fixed star [$P_{FIX}(q)$, eq 7]. The ordinate values are shifted by A for clarity.

7

Figure 5 shows molar mass dependence of $[\eta]$ for A3PQ samples in THF along with those for the corresponding linear chains. As in the case of g_s, the g_η factor defined as

$$g_\eta = \frac{[\eta]_{star}}{[\eta]_{linear}} \qquad (2)$$

was calculated with the theoretical value for the corresponding linear chain and summarized in the 8th column in Table 1. As also displayed in Figure 5, the obtained g_η values are between 4/9 and 0.90 for rigid[24] and flexible stars,[25] respectively; note that the former value is calculated for rigid stars with the fixed connection angle. Except for the lowest M_w sample, the obtained g_η values increase with increasing M_w. These features for dimensional and hydrodynamic properties strongly suggest the semiflexible nature of the current star polymer samples.
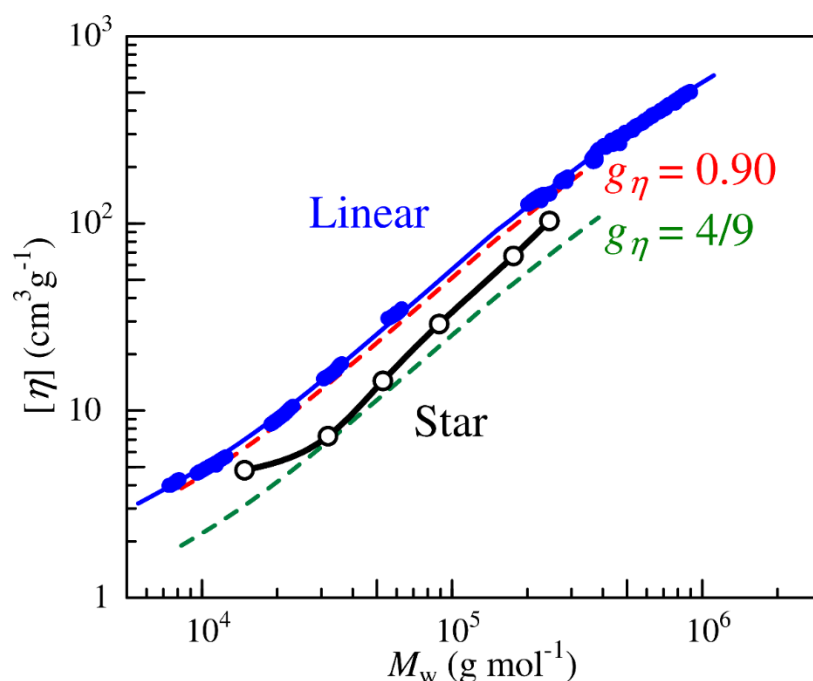

Figure 5. Double logarithmic plots of $[\eta]$ vs M_w for the A3PQ (unfilled circles) and PQX (filled circles) samples in THF at 25°C. Dashed red and green curves represent the calculated values for $g_\eta = 0.9$ and 4/9, respectively.

Discussion

Wormlike Chain Analysis of $P(q)$. Since both dimensional and hydrodynamic properties suggest the current star polymer behaves as rodlike or semiflexible stars, rod and wormlike star chain models are introduced to analyze the experimental data. According to our recent study,[14] $P(q)$ and $\langle S^2 \rangle_z^{1/2}$ data for the linear PQX were explained by the rigid rod model when $M_w < 3 \times 10^4$, suggesting that each arm of the star samples with the M_w value being less than 9×10^4 may be modeled by the rod star model. According to Huber and Burchard,[26] the scattering function $P_{BR}(q)$ of the broken three-arm rodlike star having uniform arm length L_s can be expressed as

$$P_{BR}(q) = \frac{2}{3q^2 L_s^2} \left\{ qL_s \text{Si}(qL_s) + \cos(qL_s) - 1 + \left[\text{Si}(qL_s) \right]^2 \right\} \qquad (3)$$

where Si(z) is the sine integral defined as

$$\text{Si}(z) = \int_0^z \frac{\sin t}{t} \, dt \qquad (4)$$

Each arm of this model is linked with a universal joint. The contour length L_s of each arm is one-third of the total contour length L_t, which is proportional to M_w. Thus, an M_w independent parameter h, helix pitch (or rise) per residue is defined as

$$h = \frac{L_t M_0}{M_w} = \frac{3 L_s M_0}{M_w} \qquad (5)$$

where M_0 is the molar mass of the repeat unit (= 300.2 g mol^{-1}). The chain thickness may affect $P(q)$ in the high q range. The touched bead model with the diameter d is utilized to consider this effect. The resultant scattering function $P(q)$ is expressed as

$$P(q) = 9 \left(\frac{2}{qd} \right)^6 \left(\sin \frac{qd}{2} - \frac{qd}{2} \cos \frac{qd}{2} \right)^2 P_0(q) \qquad (6)$$

where $P_0(q)$ is the particle scattering function of the thin chain; in this case, $P_{BR}(q)$. If we assume previously estimated h of 0.19 nm and $d = 0.4$ nm, the solid blue curves which are the theoretical $P(q)$ values from eq 6 with eq 3 reproduce the experimental data almost quantitatively except for the lowest and highest M_w samples. It should be noted that the chain thickness effect on $P(q)$ was invisibly small in the current q range. In order to consider the bond angle between the two arms, we also calculated the fixed rodlike star by

$$P_{FIX}(q) = \frac{2 \left[qL_s \text{Si}(qL_s) + \cos(qL_s) - 1 \right]}{3q^2 L_s^2} + \frac{2}{3L_s^2} \int_0^{L_s} ds_0 \int_0^{L_s} ds_1 \frac{\sin q\sqrt{s_0^2 + s_1^2 + s_0 s_1}}{q\sqrt{s_0^2 + s_1^2 + s_0 s_1}} \qquad (7)$$

when we choose 120° as the bond angle between arm chains. Dot-dashed red curves in Figure 4 represent the theoretical $P(q)$ for the fixed rodlike star calculated from eq 7. They clearly underestimate $P(q)$ around the peak except for the lowest M_w sample. The nicely fitted theoretical values for the lowest M_w sample may be accidental because the chain end effect as well as the core effect on $P(q)$ should be more significant for the sample. Taking into consideration that chain length distribution of side chains should make the peak lower, the broken rodlike star (eq 3) is a better model for the A3PQ samples than the fixed rodlike star.

The discrepancy between experimental and theoretical values for the highest M_w sample may be due to the finite chain flexibility. To consider this effect, the broken wormlike star model proposed by Huber and Burchard[26] was utilized in which each arm connected with a

universal joint as in the case of the broken rodlike star. In this model, the particle scattering function $P_{BW}(q)$ is expressed as

$$P_{BW}(q) = \frac{2\left[\int_0^{L_s}(L_s - t)I(\lambda^{-1}q;\lambda t)dt + \left(\int_0^{L_s}I(\lambda^{-1}q;\lambda t)dt\right)^2\right]}{3L_s^{\,2}} \tag{8}$$

Here, $I(\lambda^{-1}q;\lambda t)$ is the characteristic function of the wormlike chain, that is, the Fourier transform of the distribution function of the end-to-end distance of the wormlike chain of the contour length t and of λ^{-1}. We utilized the Nakamura-Norisuye expression[27-28] for the numerical calculation of $I(\lambda^{-1}q;\lambda t)$. The theoretical $P_{BW}(q)$ requires L_s and λ^{-1} at given q. Assuming the formally determined values, that is, $h = 0.19$ nm and $\lambda^{-1} = 43$ nm for the corresponding linear PQX, we obtained theoretical blue dashed curves in Figure 4, for which the highest M_w sample reproduce the experimental values almost quantitatively. Furthermore, theoretical values for $P_{BW}(q)$ become close to those for $P_{BR}(q)$ with lowering M_w and they quantitatively explain the experimental data except for the lowest M_w sample, supporting the above mentioned suggestion for the bond angle between the two arbitrary arms. A further important point of the result is that chain length distribution of each arm may also be narrow while it is infeasible to be determined directly.

Molar Mass dependence of Dimensional and Hydrodynamic Properties. To confirm the above mentioned conformational properties, molar mass dependence of $\langle S^2 \rangle_z^{1/2}$ was also analyzed in terms of the wormlike star models. The radius of gyration $\langle S^2 \rangle_{BW}$ for the wormlike star of which each arm is linked with a universal joint can be calculated by the Mansfield-Stockmayer scheme.[29] In the case of three-arm star, $\langle S^2 \rangle_{BW}$ is written as

$$\left\langle S^2 \right\rangle_{BW} = \frac{7L_s}{18\lambda} - \frac{5}{12\lambda^2} + \frac{3-2e^{-2\lambda L_s}}{12\lambda^3 L_s} - \frac{1-e^{-2\lambda L_s}}{24\lambda^4 L_s^{\,2}} \tag{9}$$

The g_s values for the rigid rod ($\lambda L_s \ll 1$) and the random coil ($\lambda L_s \gg 1$) are calculated to be 1/3 and 7/9, respectively. The theoretical solid curve in Figure 3 calculated from eq 9 with $h = 0.19$ nm and $\lambda^{-1} = 43$ nm fairly reproduces the experimental data. Slight underestimation is most likely due to both the molar mass distribution and arm length distribution. The dashed curve in the figure is the theoretical gyration radii $\langle S^2 \rangle_{FIX}$ values for the wormlike star with the fixed bond angle of 120°, which is also calculated by the same Mansfield-Stockmayer expression as follow

$$\left\langle S^2 \right\rangle_{FIX} = \frac{7L_s}{18\lambda} - \frac{1}{3\lambda^2} + \frac{2-e^{-2\lambda L_s}}{12\lambda^3 L_s} - \frac{1-e^{-4\lambda L_s}}{48\lambda^4 L_s^{\,2}} \tag{10}$$

The obtained theoretical values closely fit or slightly overestimate the experimental data, suggesting that the bond angle of the two arms is difficult to be estimated only from $\langle S^2 \rangle_z$.

Molar mass dependence of the Flory viscosity factor Φ

$$\Phi = \frac{[\eta]M_w}{\left(6\langle S^2 \rangle_z\right)^{3/2}} \tag{11}$$

is illustrated in Figure 6. As in the case of the corresponding linear chain, Φ decreases with increasing M_w while the absolute values are systematically larger than those for the linear chains at the same M_w. This is similar tendency for the formally investigated flexible star polymers.[30-31] Since the current theories for $[\eta]$ of the wormlike star are only available for the fixed wormlike star,[24] comparison of the experimental $[\eta]$ data with the theoretical values are not shown in this paper. It is however noted that analyses of $[\eta]$ will not give us the decisive information about the bond angle at the core because the relatively slight difference on $[\eta]$ from the bond angle restriction may be compensated by the chain thickness parameter. Indeed, if we choose $d = 2.3$ nm, the theoretical $[\eta]$ with the above mentioned h and λ^{-1} mostly fitted by the theory[24] (not shown in the figure).
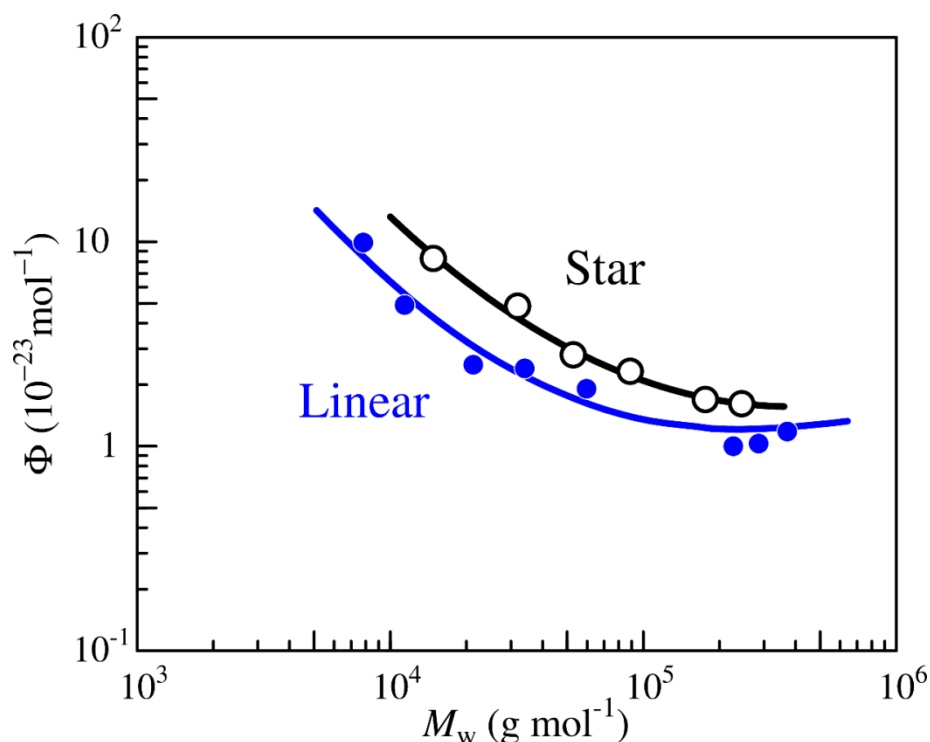

Figure 6. Double logarithmic plots of the Flory viscosity factor Φ vs M_w for A3PQ (unfilled circles) and PQX (filled circles) in THF at 25°C.

Conclusions

We synthesized three-arm star poly[5,8-dimethyl-6,7-bis(propoxymethyl)quinoxaline-2,3-diyl] (A3PQ) samples with various arm length by living polymerization using a new trifunctional palladium initiator. Solution properties characterized by the scattering function, the gyration radius, and the intrinsic viscosity were well explained by the broken wormlike star model, indicating that the arm length distribution is quite narrow and each arm connected with a rather

flexible joint. In other words, A3PQ is a well-defined star polymer with uniform arm length and suitable as a good model as rigid star polymers.

Supporting Information
Additional experimental procedures, ^{1}H NMR spectra and Single-Crystal X-Ray Analysis of trimetallic initiator 2. This material is available free of charge via the Internet at http://pubs.acs.org.

References
1.   Hadjichristidis, N.; Pitsikalis, M.; Iatrou, H.; Driva, P.; Sakellariou, G.; Chatzichristidi, M. 6.03 - Polymers with Star-Related Structures: Synthesis, Properties, and Applications A2 - Matyjaszewski, Krzysztof. In *Polymer Science: A Comprehensive Reference*, Möller, M., Ed. Elsevier: Amsterdam, 2012; pp 29-111.
2.   Nakamura, Y.; Norisuye, T. 2.02 - Polymer Properties in Solutions. In *Polymer Science: A Comprehensive Reference*, Editors-in-Chief: Krzysztof, M.; Martin, M., Eds. Elsevier: Amsterdam, 2012; pp 5-32.
3.   Yamakawa, H.; Yoshizaki, T. *Helical Wormlike Chains in Polymer Solutions, 2nd ed.* Springer: Berlin, Germany, 2016.
4.   Oka, M.; Nakajima, A. Synthesis and Characterization of Three-branched Star-like Poly(g-benzyl-l-glutamate). *Polym. Bull.* **1984,** *11*, 447-451.
5.   Goodson, S. H.; Novak, B. M. Synthesis and Characterization of Wormlike Three-arm Poly(*n*-hexyl isocyanate) Star Polymers. *Macromolecules* **2001,** *34*, 3849-3855.
6.   Kikuchi, M.; Takahara, A.; Kawaguchi, S. Dimensional Characterizations from Rod Stars to Brushes of Polymers with a Low Degree of Polymerization. *Macromolecules* **2016**.
7.   Sanada, Y.; Shiomi, T.; Okobira, T.; Tan, M.; Nishikawa, M.; Akiba, I.; Takakura, Y.; Sakurai, K. Polypod-Shaped DNAs: Small-Angle X-ray Scattering and Immunostimulatory Activity. *Langmuir* **2016,** *32*, 3760-5.
8.   Miyabe, T.; Iida, H.; Banno, M.; Yamaguchi, T.; Yashima, E. Synthesis and Visualization of a Core Cross-Linked Star Polymer Carrying Optically Active Rigid-Rod Helical Polyisocyanide Arms and Its Chiral Recognition Ability. *Macromolecules* **2011,** *44*, 8687-8692.
9.   Knoop, R. J. I.; de Geus, M.; Habraken, G. J. M.; Koning, C. E.; Menzel, H.; Heise, A. Stimuli Responsive Peptide Conjugated Polymer Nanoparticles. *Macromolecules* **2010,** *43*, 4126-4132.

10.   Skey, J.; Willcock, H.; Lammens, M.; Du Prez, F.; O'Reilly, R. K. Synthesis and Self-Assembly of Amphiphilic Chiral Poly(amino acid) Star Polymers. *Macromolecules* **2010,** *43*, 5949-5955.

11.   Siriwardane, D. A.; Kulikov, O.; Reuther, J. F.; Novak, B. M. Rigid, Helical Arm Stars through Living Nickel Polymerization of Carbodiimides. *Macromolecules* **2017,** *50*, 832-840.

12.   Ida, D. Dilute Solution Properties of Semiflexible Star and Ring Polymers. *Polym. J.* **2014,** *46*, 399-404.

13.   Terao, K.; Mizuno, K.; Bachinger, H. P. Conformational change from rigid rod to star: a triple-helical peptide with a linker domain at the C-terminal end. *J. Phys. Chem. B.* **2015,** *119*, 3714-9.

14.   Nagata, Y.; Hasegawa, H.; Terao, K.; Suginome, M. Main-Chain Stiffness and Helical Conformation of a Poly(quinoxaline-2,3-diyl) in Solution. *Macromolecules* **2015,** *48*, 7983-7989.

15.   Yamamoto, T.; Suginome, M. Helical Poly(quinoxaline-2,3-diyl)s Bearing Metal-binding Sites as Polymer-based Chiral Ligands for Asymmetric Catalysis. *Angew. Chem. Int. Ed.* **2009,** *48*, 539-42.

16.   Yamada, T.; Nagata, Y.; Suginome, M. Non-hydrogen-bonding-based, solvent-dependent helix inversion between pure P-helix and pure M-helix in poly(quinoxaline-2,3-diyl)s bearing chiral side chains. *Chem. Commun.* **2010,** *46*, 4914-6.

17.   Nagata, Y.; Yamada, T.; Adachi, T.; Akai, Y.; Yamamoto, T.; Suginome, M. Solvent-dependent Switch of Helical Main-chain Chirality in Sergeants-and-soldiers-type Poly(quinoxaline-2,3-diyl)s: Effect of the Position and Structures of the "Sergeant" Chiral Units on the Screw-sense Induction. *J. Am. Chem. Soc.* **2013,** *135*, 10104-13.

18.   Kotha, S.; Kashinath, D.; Lahiri, K.; Sunoj, Raghavan B. Synthesis of C3-Symmetric Nano-Sized Polyaromatic Compounds by Trimerization and Suzuki−Miyaura Cross-Coupling Reactions. *Eur. J. Org. Chem.* **2004,** *2004*, 4003-4013.

19.   Ito, Y.; Ohnishi, A.; Ohsaki, H.; Murakami, M. A Preparative Method foro-Diisocyanoarenes. *Synthesis* **1988,** *1988*, 714-715.

20.   Ito, Y.; Ihara, E.; Uesaka, T.; Murakami, M. Synthesis of Novel Thermotropic Liquid Crystalline Poly(2,3-quinoxalines). *Macromolecules* **1992,** *25*, 6711-6713.

21.   Berry, G. C. Thermodynamic and Conformational Properties of Polystyrene. I. Light-Scattering Studies on Dilute Solutions of Linear Polystyrenes. *J. Chem. Phys.* **1966,** *44*, 4550-4564.

22.   Grubisic, Z.; Rempp, P.; Benoit, H. A Universal Calibration for Gel Permeation Chromatography. *J. Polym. Sci. Pol. Lett.* **1967,** *5*, 753-759.

23.   Pasch, H. 2.03 - Chromatography A2 - Matyjaszewski, Krzysztof. In *Polymer Science: A Comprehensive Reference*, Möller, M., Ed. Elsevier: Amsterdam, 2012; pp 33-64.

24.   Ida, D.; Nakamura, Y.; Yoshizaki, T. Intrinsic Viscosity of Wormlike Regular Three-arm Stars. *Polym. J.* **2008,** *40*, 256-267.

25.   Irurzun, I. M. Hydrodynamic Properties of Regular Star-branched Polymer in Dilute Solution. *J. Polym. Sci., Part. B: Polym. Phys.* **1997,** *35*, 563-567.

26.   Huber, K.; Burchard, W. Scattering Behavior of Wormlike Star Macromolecules. *Macromolecules* **1989,** *22*, 3332-3336.

27.   Nakamura, Y.; Norisuye, T. Brush-Like Polymers. In *Soft Matter Characterization*, Borsali, R.; Pecora, R., Eds. Springer Netherlands: 2008; pp 235-286.

28.   Nakamura, Y.; Norisuye, T. Scattering Function for Wormlike Chains with Finite Thickness. *J. Polym. Sci., Part. B: Polym. Phys.* **2004,** *42*, 1398-1407.
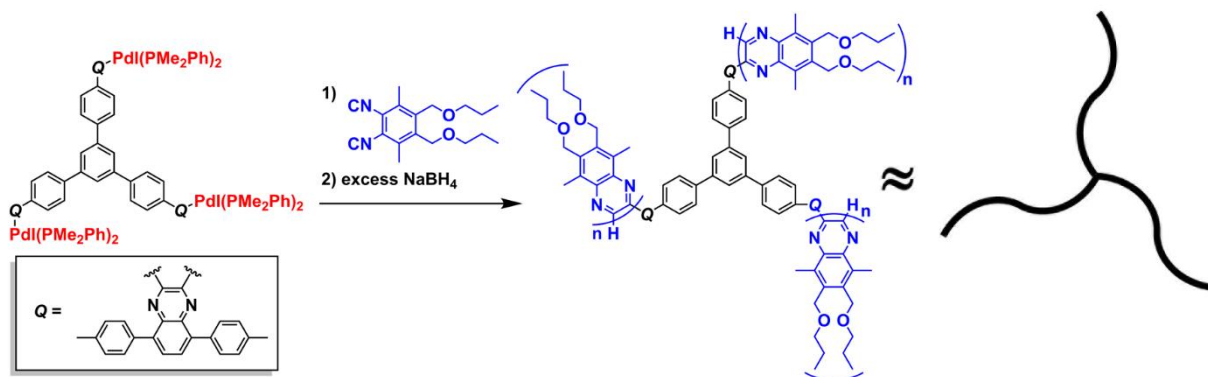
29.   Mansfield, M. L.; Stockmayer, W. H. Unperturbed Dimensions of Wormlike Stars. *Macromolecules* **1980,** *13*, 1713-1715.

30.   Roovers, J.; Toporowski, P. M. Hydrodynamic Studies on Model Branched Polystyrenes. *J. Polym. Sci., Part. B: Polym. Phys.* **1980,** *18*, 1907-1917.

31.   Okumoto, M.; Terao, K.; Nakamura, Y.; Norisuye, T.; Teramoto, A. Excluded-volume effects in star polymer solutions: Four-arm star polystyrene in cyclohexane near the Theta temperature. *Macromolecules* **1997,** *30*, 7493-7499.

For Table of Contents Use Only

Synthesis and Solution Properties of a Rigid Helical Star Polymer: Three-arm Star Poly(quinoxaline-2,3-diyl)

Hirokazu Hasegawa, Yuuya Nagata, Ken Terao, and Michinori Suginome